Environmental Science

AIMS Environmental Science, 5(2): 67–77.
DOI: 10.3934/environsci.2018.2.67
Received: 15 September 2017
Accepted: 12 March 2018
Published: 23 March 2018

http://www.aimspress.com/journal/environmental

Research article

Fluorescence detection of Zinc oxide nanoparticles in water contamination analysis based on surface reactivity with porphyrin

Wenyu Zhang and Edward P.C. Lai*

Ottawa-Carleton Chemistry Institute, Department of Chemistry, Carleton University, Ottawa, ON K1S 5B6, Canada

* **Correspondence:** Email: edward.lai@carleton.ca; Tel: +16135202600 ext. 3835; Fax: +16135203749.

Abstract: A simple rapid analytical method for determining the concentration of ZnO nanoparticles in aqueous dispersion has been developed by adding porphyrin (TCPP) as a fluorophore into the water sample for fluorescence analysis. Quenching of the emission intensity at 650 nm provides a Stern-Volmer plot with adequate sensitivity for the detection of ZnO nanoparticles from 0.15 mg/mL up to 1.5 mg/mL. A new emission peak at 605 nm can be attributed to the formation of a unique ZnO-TCPP complex. This unique emission peak is good for both identification and quantitation of ZnO nanoparticles at low concentrations down to 0.0015 mg/mL. The new method affords a linear dynamic range up to 1.2 mg/mL.

Keywords: fluorescence; nanoparticles; porphyrin; quenching; Stern-Volmer; water contamination analysis; zinc oxide

1. Introduction

Nanomaterials exhibit novel physicochemical properties that determine their application in various industrial manufacturing processes. Three metal oxide nanoparticles namely titania (TiO_2), zinc oxide (ZnO), and ceria are produced in high tonnages for use as additives in nanomaterials. ZnO nanoparticles are a widely used ingredient of cosmetics. They have a wide range of antibacterial activities toward various Gram-positive and -negative microorganisms [1] and could be developed as antibacterial agents to control and prevent the spreading of persistent bacterial infections. Unfortunately, ZnO nanoparticles can induce toxicity in biological cells leading to the generation of reactive oxygen species, oxidant injury,

excitation of inflammation, and cell death [2]. Their induction of cell death and carcinogenesis depends on the endogenous genetic, transcriptomic and proteomic landscape of the target cells [3]. Oral exposure to ZnO nanoparticles in mice leads to an accumulation of nanoparticles in the liver causing oxidative stress mediated DNA damage and apoptosis [4]. The nanoparticles also possess a genotoxic potential in human epidermal cells even at low concentrations [5].

Fluorescent nanoparticles are widely used for the purpose of bioimaging cells and tissues. Compared to molecular fluorophores, fluorescent nanoparticles offer many meritorious features [6]. Two fluorescence maxima were observed for ZnO particles—the bandgap fluorescence at 365 nm and the visible luminescence at 520 nm—with a low overall fluorescence quantum yield of 0.03 [7]. Intrinsically fluorescent ZnO nanowires (NWs) were adopted for molecularly targeted imaging of cancer cells, after they were functionalized to render water solubility, biocompatibility, and low cellular toxicity [8]. ZnO nanoparticles were conjugated with a hydroxysuccinimide ester of Cy5.5 to investigate their accumulation in rats using optical imaging after oral exposure [9]. Combining ZnO nanoparticles and ammonia gas increased the photoluminescent intensity of the ZnO nanoparticles, thereby showing their tremendous applicability in optical sensors for the detection of ammonia gas [10]. Quenching of the visible emission of ZnO colloid particles was reported for ferricyanide, ferrocyanide and chloroplatinate anions in the presence of polybrene [11]. The fluorescence of bovine serum albumin conjugated ZnO nanoparticles could be quenched selectively by Cu^{2+} ions in physiological buffer solution. The quenching was static with a rate constant of 7×10^{12} L mol^{-1} s^{-1} [12]. ZnO nanorods have a bimodal photoluminescence spectrum that consists of an ultraviolet excitonic peak and a visible surface-defect-related peak. The intensities of both UV and visible peaks were decreased due to quenching by covalently linked gold nanoparticles [13].

Surface catalytic reactivity of nanoparticles could be applied to detect the type and concentration of nanoparticles with limit of detection down to part per million [14]. ZnO nanoparticles could be detected by capillary electrophoresis (CE) coupled with UV detection after adsorption of dithiothreitol (DTT) or cysteine (Cys) [15]. However, in this work, a quantitative fluorescence method is developed for the analysis of ZnO nanoparticles in water. Porphyrins are a group of heterocyclic compounds that occur in nature with several important biochemical properties. Each porphyrin molecule is composed of four pyrrole rings connected by methylene bridges to α-carbon atoms, forming an aromatic macrocycle structure [16]. Free base porphyrins are recognized to have stable interactions with a wide range of metal cations to produce intense absorption bands in the UV to visible spectral region [17]. This also provides a good opportunity of fluorescence detection by specific adsorption of porphyrin onto ZnO nanoparticles to afford a low detection limit towards 1 μg/mL in water contamination analysis.

2. Method and materials

2.1. Materials

Methanol was purchased from VWR (Mississauga, ON, Canada). Meso-tetra(4-carboxyphenyl)porphyrin (H_2TCPP) and all metal oxide nanopowders Al_2O_3 (<50 nm particles size), CuO (<50 nm particles size), CeO_2 (<50 nm particles size), TiO_2 (21 nm particles) and ZnO (<50 nm particles size) were obtained from Sigma-Aldrich (Oakville, ON, Canada). Zinc acetate was purchased from Fisher Scientific Company (USA).

2.2. Sample preparation

2 mg of H_2TCPP was dissolved in 20 mL of methanol. The stock solution of ZnO nanoparticles (1.5 mg/mL) was prepared by dispersing 15 mg of ZnO in 10 mL of methanol using an ultrasonic processor (WQY 064). Serial concentrations of ZnO nanoparticles were prepared in methanol from 0.0 to 1.5 mg/mL (see Table 1) for testing them as a quencher of the fluorescence emission from H_2TCPP. To determine the time-dependent quenching effect, the same batch of samples were stored on standing at 298 K for different days before analyzing. The interference effect of TiO_2 nanoparticles was prepared by dispersing serial concentrations of TiO_2 nanoparticles from 0.0 to 0.5 mg/mL (Table 2) in constant concentration of ZnO nanoparticles.

Table 1. Concentration of ZnO nanoparticles for porphyrin (TCPP) quenching.

Sample ID	0	1	2	3	4	5	6	7	8	9	10	11
Concentration (mg/mL)	0	0.15	0.225	0.3	0.45	0.6	0.75	0.9	1.05	1.2	1.35	1.5
ZnO stock (mL)	0	0.1	0.15	0.2	0.3	0.4	0.5	0.6	0.7	0.8	0.9	1
Methanol (mL)	1	0.9	0.85	0.8	0.7	0.6	0.5	0.4	0.3	0.2	0.1	0
H_2TCPP (μL)	400	400	400	400	400	400	400	400	400	400	400	400

Table 2. Concentration of ZnO nanoparticles and TiO2 nanoparticles for TiO2 interference analysis.

Sample ID	0	1	2	3	4	5
Concentration of ZnO (mg/mL)	0.5	0.5	0.5	0.5	0.5	0.5
Concentration of TiO_2 (mg/mL)	0	0.1	0.2	0.3	0.4	0.5
H_2TCPP (μL)	400	400	400	400	400	400

2.3. UV-visible spectroscopy

Zn-TCPP was prepared by adding 400 μL of porphyrin stock solution to 1 mL of 0.01M Zinc Acetate as a comparison. Absorption spectra were measured on a Thermo Scientific GENESYS 10S UV-vis spectrophotometer with a slit width of 1.0 nm.

2.4. Spectrofluorometry

Metal oxide dispersion (0.75 mg/mL, 1 mL) was mixed with 400 μL of H_2TCPP solution (1 mg/mL). Metal oxide-porphyrin (200 μL) and 2 mL of methanol were added into a 1-cm quartz cuvette. The fluorescence intensity was recorded while the emission wavelength was scanned from 550 nm to 750 nm with fixed excitation of 420 nm using a FluoroMax-4 spectrofluorometer (Horiba Scientific).

3. Results and discussion

3.1. UV-visible spectroscopy

In Figure 1, the UV-vis absorption spectrum of free base porphyrin (TCPP) shows a Soret band at 414 nm and four Q bands at 514 nm, 548 nm, 590 nm, and 646 nm. The UV-vis absorption of ZnO nanoparticles in methanol exhibited a peak at 360 nm. Porphyrin-coated ZnO nanoparticles showed a combination of ZnO absorption peak at 357 nm and a red-shifted porphyrin Soret band at 421 nm (Figure 1a). Porphyrin can react with zinc acetate to form the Zn-TCPP complex (or conjugate) where a zinc ion binds to the center of porphyrin. The UV-vis spectrum of Zn-porphyrin exhibits a Soret band that overlaps with the 421 nm band of porphyrin-coated ZnO nanoparticles [18], which indicated a chemical interaction of the porphyrin coating with the ZnO nanoparticles. In Figure 1b, the magnification of wavelength from 450 to 700 nm also indicates a red-shift of 2–4 nm on all four Q bands of Zn-TCPP [19].

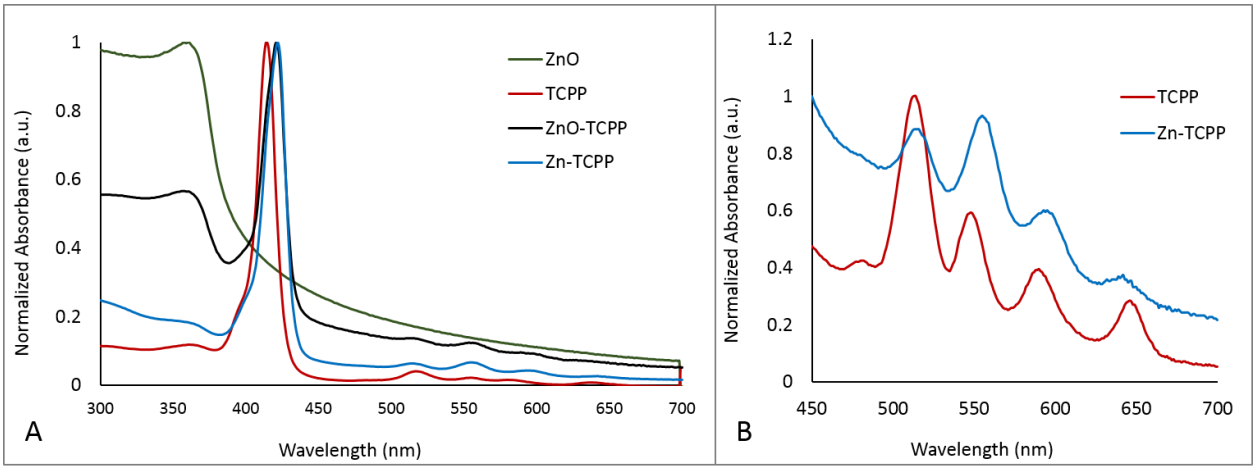

Figure 1. (A) Normalized UV-visible absorption spectrum of ZnO nanoparticles, porphyrin, porphyrin-coated ZnO and Zn-porphyrin in methanol; (B) Magnification of Q-bands of porphyrin and Zn-porphyrin from 450 nm to 700 nm.

3.2. Fluorescence spectroscopy

Among five metal oxide nanoparticles (Al_2O_3, CeO_2, CuO, TiO_2 and ZnO) tested for porphyrin quenching, ZnO has the highest quenching efficiencies to both peaks at ~650 nm and ~710 nm (Figure 2a). From the data in Figure 2a, it appears that divalent metal oxides (ZnO and CuO) are better quenchers than trivalent metal oxide (Al_2O_3) and tetravalent metal oxides (TiO_2 and CeO_2). In addition, the interaction between ZnO nanoparticles and porphyrin raises a new peak at 605 nm, which gives zinc oxide a unique fluorescence emission compared to other metal oxide nanoparticles. To identify the source of emission peak at 605 nm from porphyrin-coated ZnO nanoparticles, the fluorescence emission of Zn-TCPP also showed a peak with nearly identical wavelength at ~607 nm. Thus, this peak at 605 nm is unique for Zinc ion and ZnO nanoparticles due to the electron transfer between metal and the porphyrin π-system [20]. Moreover, the fluorescence emission of Zn-TCPP had a

significant red shift from 647 nm to 654 nm compared with that of porphyrin [21]. Upon adding ZnO nanoparticles, the intense pink color of porphyrin faded and became pale yellow (Figure 2c). With excess of Zn^{2+} and ZnO adding to H_2TCPP, the emission spectra showed an overlap of the peaks at ~607 nm after normalization (Figure 2b).

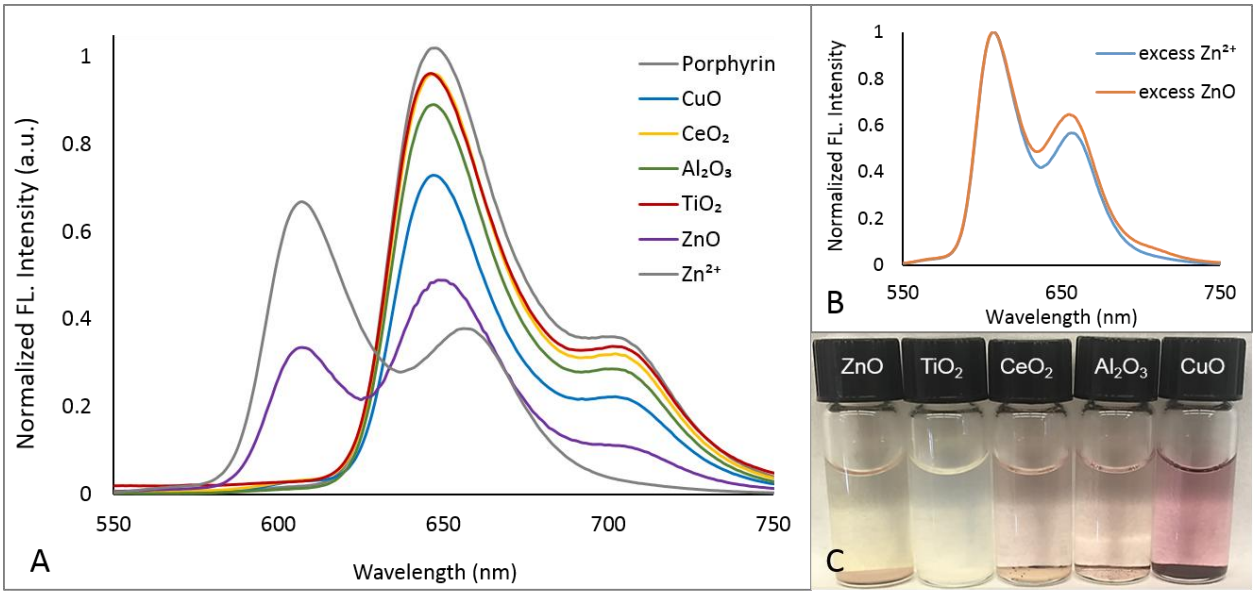

Figure 2. Fluorescence emission spectra using an excitation wavelength of 420 nm: (A) porphyrin and its quenching by Zn^{2+} and different metal oxide nanoparticles (CuO, CeO_2, Al_2O_3, TiO_2 and ZnO) at the same mass concentration of 1.5 mg/mL, and (B) porphyrin with excess Zn acetate and ZnO nanoparticles in PBS buffer. (C) Colour change of porphyrin in presence of different metal oxide nanoparticles.

3.3. Detection of ZnO by quenching effect

The fluorescence intensity of porphyrin decreased at a wavelength of ~650 nm (green arrow in Figure 3) as the concentration of ZnO quencher increased from 0.15 mg/mL to 1.5 mg/mL. The fluorescence intensity of porphyrin also decreased at ~710 nm (blue arrow) and finally diminished when the concentration of ZnO reached 1.35 mg/mL [19]. Meanwhile, the fluorescence intensity originating from the interaction between ZnO and porphyrin continued to increase the fluorescence intensity of a new peak at 605 nm (red arrow). Similar quenching of TCPP fluorescence and a slightly increasing peak at 605 nm had previously been reported by Jones et al. for Zn^{2+} produced from photoetching ZnO nanopowder solution under UV irradiation [22]. Most importantly, it is evident that the 605 nm peak increased its intensity faster than the fluorescence quenching of both the 650 and 710 nm peaks to offer enhanced detection sensitivity.

3.4. Calibration curve of Stern-Volmer plot

The calibration curve of fluorescence intensity and quencher concentration can be best expressed by the Stern-Volmer equation which usually gives a linear relationship [23]:

$$I_0/I = 1 + K_{sv}[Q] \quad (1)$$

where I_0 is the maximum fluorescence intensity in the absence of quencher, I is the maximum intensity when quencher is present, K_{sv} is the Stern-Volmer constant, and [Q] is the concentration of quencher. The linear range of the Stern-Volmer plot is from 0.05–1.2 mg/mL with a K_{sv} value of 0.66 mL/mg. However, the Stern-Volmer plot of low concentration ZnO nanoparticles quenching porphyrin exhibits a high overall quenching effect trend, as the incubation time has significant influence to quenching effects, which will be explained in detail in next section (Figure 4).

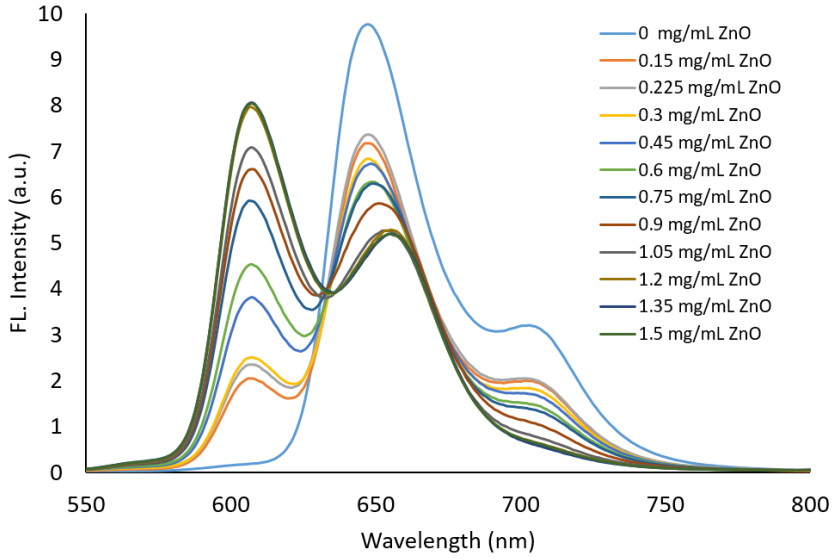

Figure 3. Fluorescence emission spectra of porphyrin (TCPP) with different concentrations of ZnO nanoparticles, using an excitation wavelength of 420 nm.

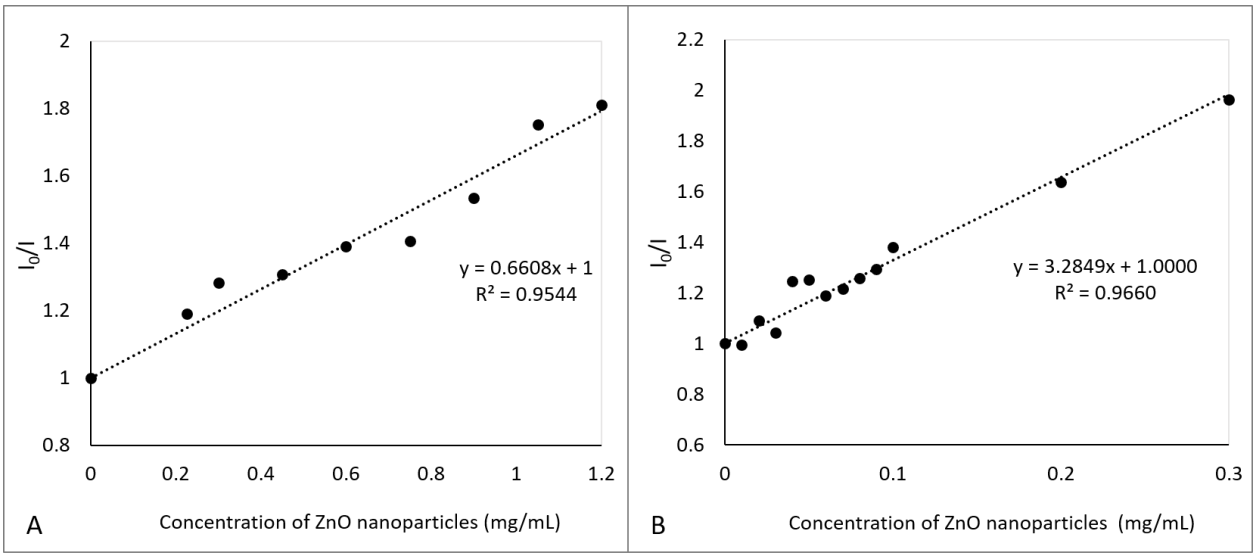

Figure 4. Stern-Volmer plot for porphyrin (TCPP) at (a) medium concentrations and (b) low concentration of ZnO nanoparticles, using excitation wavelength of 420 nm and maximum emission wavelength.

3.5. Time-dependent quenching

The kinetic rate of complex formation between TCPP and ZnO nanoparticles is relatively slow especially for low concentrations. Overnight reaction affords only a modest I_0/I result after 1 day. However, the fluorescence intensity of TCPP decreases continuously with increasing reaction time especially at ZnO nanoparticle concentrations lower than 0.1 mg/mL, which results in an increase of the corresponding I_0/I value (Figure 5). Therefore, the Stern-Volmer constant (K_{sv}) experiences a significant increase with reaction time and can be modelled in a second-order polynomial function with an R^2 value greater than 0.99 (Figure 5b). A similar second-order polynomial relationship between K_{sv} and reaction time was reported in a previous work [24]. Although greater K_{sv} can provide a more sensitive calibration curve, the shortened linear dynamic range from 0.7 mg/mL to 0.1 mg/mL will not provide an accurate determination (Figure 5a) unless the unknown sample is diluted to repeat the fluorescence intensity measurement. The macrocycle strain effect of porphyrin structures on the complex formation rate with zinc was previously studied by Simonova et al. They optimized the molecular structure of porphyrin by the PM3 quantum-chemical method in order to obtain the best complex formation rate [25].

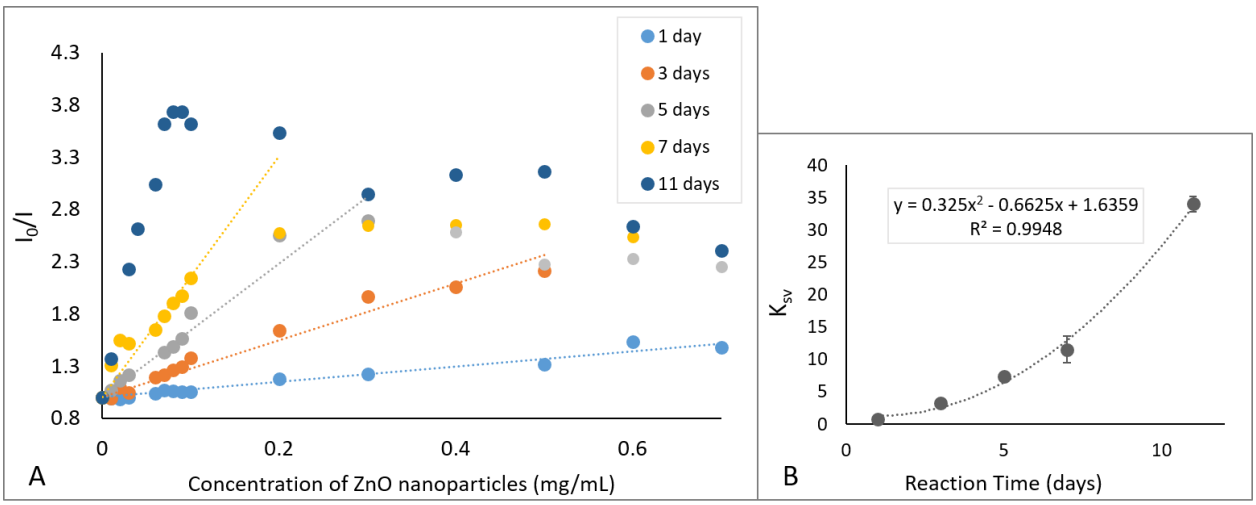

Figure 5. (a) Stern-Volmer plots on different days after mixing porphyrin (1 mg/mL) with different concentrations of ZnO nanoparticles (0.0 to 0.7 mg/mL); (b) Stern-Volmer constant (obtained from figure 5a) versus reaction time, using excitation wavelength of 420 nm and maximum emission wavelength.

3.6. Direct fluorescence emission from ZnO-TCPP

The unique peak at 605 nm from ZnO-TCPP complex was utilized for the quantitative analysis of ZnO nanoparticles by direct fluorescence emission (rather than quenching). A plot of maximum intensities at 605 nm versus different concentrations of ZnO nanoparticles displayed a linear regression fit (Figure 6). For 1 mg/mL porphyrin, the linear dynamic range is up to 1.2 mg/mL ZnO nanoparticles; the detection limit is 0.0015 mg/mL, where the unique peak at 605 nm is not distinguishable from the broad shoulder (based on the average blank signal + 3∗standard deviation).

The limit of detection is at the scale of former reported detection method to ZnO nanoparticles and will be efficient to 1000-fold pre-concentrated environmental surface water, regarding that the reported hypothetical concentration is approximately 1×10^{-5} mg/mL [15,26]. This direct fluorescence measurement is more useful in unknown water analysis, as the appearance of a peak at 605 nm has very high selectivity and sensitivity in detection of ZnO nanoparticles.

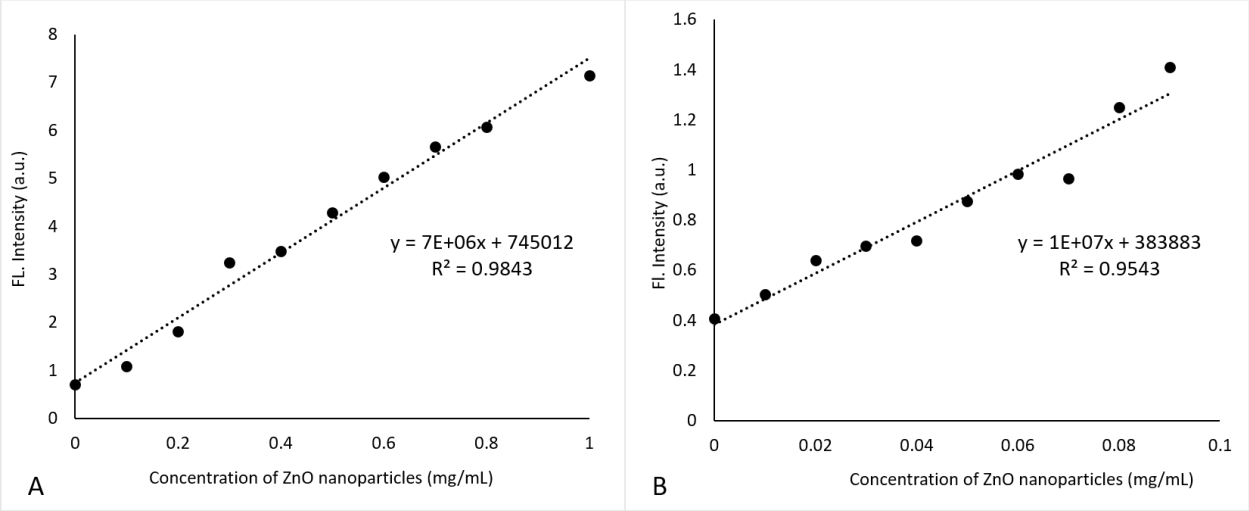

Figure 6. Fluorescence intensity of ZnO-TCPP complex at (a) medium concentrations and (b) low concentrations of ZnO nanoparticles, using excitation wavelength of 420 nm and maximum emission wavelength of 605 nm.

3.7. ZnO in mixture with TiO2 nanoparticles

To determine the interference of other metal oxide nanoparticles with porphyrin quenching by ZnO nanoparticles, two mixtures were prepared with and without ZnO nanoparticles. The color of porphyrin becomes pale yellow with the presence of ZnO in the mixture of metal oxide nanoparticles (Figure 7a), which indicates the presence of ZnO nanoparticles because ZnO is the only one can diminish porphyrin color among five metal oxides. The fluorescence emission spectra shows an obvious peak at 605 nm in ZnO sample comparing to that of no ZnO added sample which has a flat shoulder in the correspond area (Figure 7a). The interference test with serial concentration of TiO_2, one of common used nanoparticles with relatively high affinity to porphyrin, shows no trend in neither the Stern-Volmer quenching plot nor the direct fluorescence method (Figure 7b). Overall, even in the presence of TiO_2 nanoparticles, the unique emission peak at 605 nm can selectively determine the presence and concentration of ZnO nanoparticles.

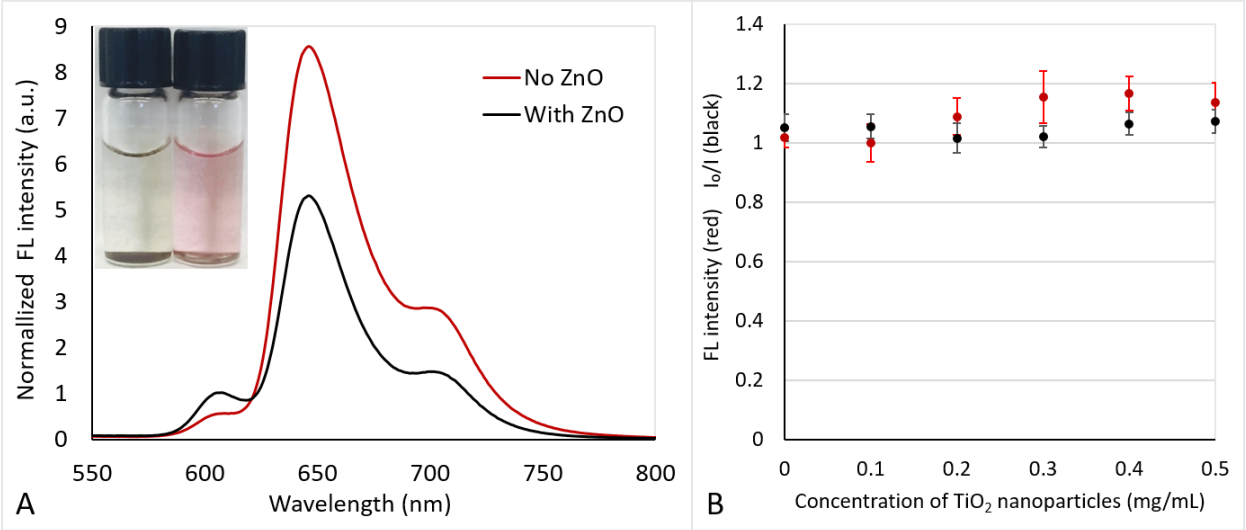

Figure 7. (a) Fluorescence emission spectra of porphyrin with a mixture of metal oxides in the presence and absence of ZnO nanoparticles. (b) Fluorescence intensity at 605 nm (red) and Stern-Volmer plot (black) of interference test with serial concentrations of TiO_2 nanoparticles.

3.8. Effect of pH on direct fluorescence emission from ZnO-TCPP

In the case of ZnO nanoparticles, the predominant effect of pH is for dissolution and aggregation level of nano-structure. The dispersion of ZnO nanoparticles in water normally results pH 7.7, which is considered at a stable pH for ZnO with not much Zn^{2+} leaking from nanoparticles. Their solubility limit is close to pH ~8.2 but nearly complete dissolution occurs at pH 4.8–6.5 [27]. This pH dependency of ZnO nanoparticles dissolution can be utilized to differentiate them from Zn^{2+} in an unknown water sample. If the direct fluorescence emission intensity of ZnO-TCPP is first measured and then the sample pH is adjusted to 4.8 using acetic acid/sodium acetate buffer, the dissolution of ZnO nanoparticles will produce significant concentration of Zn^{2+} to enhance the emission intensity significantly at 605 nm. This intensity enhancement is directly proportional to the concentration, but inversely correlated with the size, of ZnO nanoparticles. Alternatively, centrifugation of the water sample can remove dissolved Zn^{2+} first. Then the pellet can be re-dissolved in the acetate buffer to produce Zn^{2+} which is useful to rapid quantification with TCPP.

4. Conclusion

We have developed an analytical method for determining the contamination of water by ZnO nanoparticles. The method is initially based on the quenching of fluorescence emission from porphyrin (TCPP) that acts as a fluorophore. ZnO nanoparticles have high quenching efficiency to generate a Stern-Volmer plot that provides sensitive detection at low concentrations (0.1 mg/mL). Interestingly, the quenching efficiency increases with time and temperature which can be optimized to further improve the detection limit in water contamination analysis. Unlike other metal oxide nanoparticles, ZnO nanoparticles produce a unique emission peak at 605 nm that is attributed to the

formation of a ZnO-TCPP complex. This unique emission peak can be used for both identification and quantitation of ZnO nanoparticles, without any significant interference by TiO_2 nanoparticles. Other divalent metal oxide (CaO, MgO and SnO) nanoparticles can be studied in the future to evaluate their potential interference with the unique ZnO peak produced by the complexation of ZnO with TCPP.

Acknowledgment

Financial support from NSERC Canada (grant number 315574) is gratefully acknowledged.

Conflict of interest

The authors declare there is no conflict of interest.

References

1. Raghupathi KR, Koodali RT, Manna AC (2011) Size-dependent bacterial growth inhibition and mechanism of antibacterial activity of zinc oxide nanoparticles. *Langmuir* 27: 4020–4028.
2. Xia T, Kovochich M, Liong M, et al. (2008) Comparison of the mechanism of toxicity of zinc oxide and cerium oxide nanoparticles based on dissolution and oxidative stress properties. *ACS Nano* 2: 2121–2134.
3. Ng KW, Khoo SPK, Heng BC, et al. (2011) The role of the tumor suppressor p53 pathway in the cellular DNA damage response to zinc oxide nanoparticles. *Biomaterials* 32: 8218–8225.
4. Sharma V, Singh P, A.K. Pandey AK, et al. (2012) Induction of oxidative stress, DNA damage and apoptosis in mouse liver after sub-acute oral exposure to zinc oxide nanoparticles. *Mutat Res-Gen Tox En* 745: 84–91.
5. Sharma V, Shukla RK, Saxena N, et al. (2009) DNA damaging potential of zinc oxide nanoparticles in human epidermal cells. *Toxicol Lett* 185: 211–218.
6. Wolfbeis OS (2015) An overview of nanoparticles commonly used in fluorescent bioimaging. *Chem Soc Rev* 44: 4743–4768.
7. Bahnemann DM, Korman C, Hoffmann MR (1987) Preparation and characterization of quantum size zinc oxide—a detailed spectroscopic study. *J Phys Chem* 91: 3789–3798.
8. Hong H, Shi J, Yang Y, et al. (2011) Cancer-targeted optical imaging with fluorescent zinc oxide nanowires. *Nano Letters* 11: 3744–3750.
9. Lee CM, Jeong HJ, Yun KN, et al. (2012) Optical imaging to trace near infrared fluorescent zinc oxide nanoparticles following oral exposure. *Int J Nanomedicine* 7: 3203–3209.
10. Singh N, Syed F, Haque FZ (2014) Ionic liquid controlled growth of zinc oxide nanoparticles and their fluorescence study in the presence of NH3 gas. *Mater Sci Res India* 11: 27–34.
11. Rabani J, Behar D (1989) Quenching of aqueous colloidal zinc oxide fluorescence by electron and hole scavengers—effect of a positive polyelectrolyte. *J Physic Chem* 93: 2559–2563.
12. Chen Z, Wu D (2014) Monodisperse BSA-conjugated zinc oxide nanoparticles based fluorescence sensors for Cu^{2+} ions. *Sensor Actuat B-Chem* 192: 83–91.
13. Unlu I, Soares JW, Steeves DM, et al. (2015) Photocatalytic activity and fluorescence of gold/zinc oxide nanoparticles formed by dithiol linking. *Langmuir* 31: 8718–8725.

14. Corredor C, Borysiak MD, Wolfer J, et al. (2015) Colorimetric Detection of Catalytic Reactivity of Nanoparticles in Complex Matrices. *Environ Sci Technol* 49: 3611−3618.
15. Alsudir S, Lai EPC (2017) Selective detection of ZnO nanoparticles in aqueous suspension by capillary electrophoresis analysis using dithiothreitol and L-cysteine adsorbates. *Talanta* 169: 115–122.
16. Biesaga M, Pyrzyńska K, Trojanowicz M (2000) Porphyrins in analytical chemistry. A review. *Talanta* 51: 209–224.
17. Gouterman M (1961) Spectra of porphyrins. *J Mol Spectrosc* 6: 138–163.
18. Aly SMB, Eita M, Khan JI, et al. (2014) Remarkable fluorescence enhancement versus complex formation of cationic porphyrins on the surface of ZnO nanoparticles. *J Physic Chem* 118: 12154−12161.
19. Hiromitsu I, Kawami A, Tanaka S, et al. (2011) Luminescence of tetraphenylporphyrin by an energy transfer from photoexcited ZnO nanoparticles. *Chem Phys Lett* 501: 385−389.
20. Harriman A (1980) Luminescence of porphyrins and metalloporphyrins. Part 1-Zinc(II), nickel(II) and manganese(II) porphyrins. *Journal of the Chemical Society, Faraday Transactions 1: Physical Chemistry in Condensed Phases* 76: 1978–1985.
21. Penon O, Moro AJ, Santucci D, et al. (2014) Molecular recognition of aliphatic amines by luminescent Zn-porphyrins. *Inorganica Chimica Acta* 417: 222–249.
22. Jones P, Sugino S, Yamamura S, et al. (2013) Impairments of cells and genomic DNA by environmentally transformed engineered nanomaterials. *Nanoscale* 5: 9511–9516.
23. Kang J, Wu H, Lu X, et al. (2005) Study on the interaction of new water-soluble porphyrin with DNA. *Spectrochim Acta A* 61: 2041–2047.
24. Xi G, Wang X, Chen T (2016) A reduced graphene oxide-based fluorescence resonance energy transfer sensor for highly sensitive detection of matrix metalloproteinase 2. *Inte J Nanomedicine* 11: 1537–1547.
25. Simonova OR, Zaitseva SV, Koifman OI (2008) Effect of the porphyrin structure on the kinetics of complex formation with zinc dipyrromethene in dimethylformamide. *Russ J Inorg Chem* 53: 391–396.
26. Gagne F, Auclair J, Trepanier S, et al. (2016) The impact of zinc oxide nanoparticles in freshwater mussels exposed to municipal effluents. *Invertebr Surviv J* 13: 281–290.
27. Odzak N, Kistler D, Sigg L (2017) Influence of daylight on the fate of silver and zinc oxide nanoparticles in natural aquatic environments. *Environ Pollut* 226: 1−11.

AIMS Press